Phenyl-substituted fluorene-dimer cored anthracene derivatives: highly fluorescent and stable materials for high performance organic blue- and white-light-emitting diodes†

Shanghui Ye,[ab] Jianming Chen,[ab] Chong-an Di,[a] Yunqi Liu,*[a] Kun Lu,[ab] Weiping Wu,[ab] Chunyan Du,[ab] Ying Liu,[ab] Zhigang Shuai[c] and Gui Yu[a]

Received 3rd December 2009, Accepted 29th January 2010
First published as an Advance Article on the web 1st March 2010
DOI: 10.1039/b925418h

A new series of highly fluorescent blue-emitting materials based on fluorene and anthracene hybrids are designed and synthesized for organic light-emitting diodes (OLEDs). These materials feature a phenyl-substituted fluorene dimer as a bulky and rigid core and anthracene as a functional active group. The novel use of a phenyl-substituted fluorene dimer as building skeleton to design functional molecules is reported for the first time. The thermal, photophysical, electrochemical, and electroluminescent (EL) properties are presented, as well as combined density functional study of their geometry and electronic structure. These compounds show excellent thermal resistance with high glass transition temperature (T_g) in the range 159–257 °C, thermal decomposition temperature (T_d) 441–495 °C, and high fluorescent quantum yield (Φ_F = 0.61–0.96, relative to 9,10-diphenylanthracene) as well as good film-forming and morphological stability. Remarkably, high-performance blue OLEDs are also fabricated in a simple three-layer device architecture using these compounds as emissive layer with luminance efficiency of 2.2–5.1 cd A^{-1} as a non-doped blue emitter and even higher efficiency of up to 13.6 cd A^{-1} and maximum external quantum efficiency 4.8% is obtained when doped a blue fluorescent dye, 4,4′-(1*E*,1′*E*)-2,2′(biphenyl-4,4′diyl)bis(ethane-2,1-diyl)bis(*N*,*N*-di*p*-tolyaniline) (DPAVBi). Furthermore, we fabricate highly efficient fluorescent white OLEDs employing an interesting emission in the longer wavelength of one of our compound combined with DPAVBi emission to achieve stable white light emission in a binary blend single emissive layer with high efficiency of 14.8 cd A^{-1} (5.3 lm W^{-1}) and maximum brightness of 50248 cd m^{-2}.

1. Introduction

Since the first report by Tang *et al.*, organic light-emitting diodes (OLEDs), whether based on small molecules or polymers, have been made dramatic progress because of their potential applications in full-color flat-panel display and solid-state illumination sources.[1,2] Among the three primary colors, although green- and red-emitting diodes have been approached the practical requirement,[3–6] blue-emitting diodes remain relatively poor due to their intrinsic characteristics such as wide band-gap, low lying the highest occupied molecular orbit (HOMO) energy levels, and thus high carrier injection barrier into the emitter. It remains a great challenge to develop highly efficient blue-emitting diodes with stable and good color purity. Many materials have been synthesized in the development of blue OLEDs, such as distyrylarylene derivatives (DSA),[7–9] hydroxyphenyl-pyridine beryllium complex,[10] bistriphenylenyl,[11] fluorenes–especially spirofluorenes-cored conjugated compounds,[12–16] anthracene derivatives,[17–23] and fluorene/anthracene hybrids.[24–27] Very recently, Lyu *et al.*[28] developed a series of new silicon-cored anthracene derivatives by non-conjugated connecting two anthracene units through a silicon-core. These compounds exhibit high glass transition temperatures (T_g) range from 102 to 177 °C and bright blue emission with high color purity and a high efficiency up to 7.5 cd A^{-1} with an emission peak at 460 nm in a doped device configuration. Although many blue-light emitters have been reported, highly efficient ones exhibiting high thermal stability and robust emission are still rare.

Anthracene derivatives have been extensively explored in fabrication of highly efficient and stable OLEDs, mainly due to their high photoluminescence (PL) quantum yield, electroluminescence (EL) properties, and good electrochemical properties.[29] Among these anthracene derivatives, 9,10-di(naphthalene-2-yl)anthracene (ADN) is one of the most representative blue fluorescent materials for its fluorescence properties and thermal stability.[30] However, they fail to provide dense films or the vapor-deposited thin films tend to crystallize, resulting in rough surface, grain boundaries or pin holes that lead to current leakage or catastrophic device failure.[24,31] In general, amorphous thin films having high T_g are less vulnerable to heat and thence their devices

[a]*Key Laboratory of Organic Solids, Institute of Chemistry, Chinese Academy of Sciences, Beijing 100190, P. R. China. E-mail: liuyq@iccas.ac.cn*
[b]*Graduate School of Chinese Academy of Sciences, Beijing 100084, P. R. China*
[c]*Department of Chemistry, Tsinghua University, Beijing 100084, P. R. China*

† Electronic supplementary information (ESI) available: UV–vis absorption spectra of DAPFB, DPAPFB, and DNAPFB thin films on quartz slice. Cyclic voltammogram of DAPFB, DPAPFB, and DNAPFB. See DOI: 10.1039/b925418h

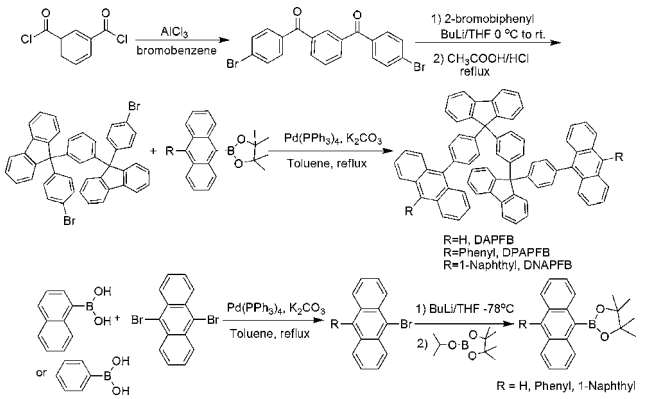

Scheme 1 Synthetic route of the three target products and the corresponding intermediates.

perform more stably.[32] Consequently, light-emitting materials possessing high values of T_g are desired to retain the film morphology during the operation of the device.

In the previously study, we and others have demonstrated that incorporating a rigid and bulky tetrahedral molecular skeleton, such as fluorene and carbazole, into a molecule can improve its film-forming and morphologically stability through the non-conjugated linking method to pursue high-triplet-energy blue phosphorescent host materials.[33–36] Although fluorene is a well-known building block, the novel use of phenyl-substituted fluorene dimer as a building skeleton to design functional molecules is never reported. In this contribution, we firstly report the use of a phenyl-substituted fluorene dimer as a bulky and rigid core to design functional materials. A new series of blue light-emitting materials, 1,3-bis(9-(4-(anthracen-9-yl)phenyl)-9*H*-fluoren-9-yl)benzene (DAPFB, Scheme 1), 1,3-bis(9-(4-(10-phenylanthracen-9-yl)phenyl)-9*H*-fluoren-9-yl)benzene (DPAPFB), and 1,3-bis(9-(4-(10-(naphthalen-1-yl)anthracen-9-yl)phenyl)-9*H*-fluoren-9-yl)benzene (DNAPFB), which features anthracene as the functional active group and the phenyl-substituted fluorene dimer as the bulky and rigid core. These compounds connected through the sp^3-hybridized carbon atom at C–9 position of the fluorene, which serves as a spacer to effectively block conjugation between them, thus individual unit's photophysical and electrochemical properties are remained unperturbed. Moreover, the resulting molecules have a sterically bulky 3D cardo structure, which not only hinders their close packing and crystallization but also increases their molecular rigidity, leading to amorphous materials having pronounced morphological stability. In a simple three-layer device architecture these compounds show respectable high luminance efficiency of about 2.2–5.1 cd A^{-1} as a blue emitter and an even higher efficiency of up to 13.6 cd A^{-1} of DPAPFB based blue OLEDs and 14.8 cd A^{-1} of DNAPFB based white OLEDs when doped with a blue fluorescent dopant, 4,4′-(1*E*,1′*E*)-2,2′(biphenyl-4,4′diyl)bis(ethane-2,1-diyl)bis(*N*,*N*-di*p*-tolyaniline) (DPAVBi).

2. Result and discussion

2.1. Material synthesis

The synthetic routes and chemical structures of DAPFB, DPAPFB, and DNAPFB are shown in Scheme 1. Friedel–Crafts benzoylation of isophthaloyl dichloride and bromobenzene gives the 1,3-bis(4-bromobenzoyl)benzene, which was treated with biphenyl-2-yllithium followed by cyclization to produce 1,3-bis(9-(4-bromophenyl)-9*H*-fluoren-9-yl)benzene (DBPFB). Suzuki coupling reactions of DBPFB with the corresponding anthryl boronic ester in the presence of a catalytic amount of $Pd(PPh_3)_4$ and 2 M K_2CO_3 yields the target products. We chose Friedel–Crafts benzoylation and cyclization routes to produce defect-free 9,9-diarylfluorene, inspired by the recent studies demonstrated by Holmes *et al.* that the structural perfection of fluorene-based light-emitting materials depends on the synthetic route of the monomers.[37] We use isophthaloyl dichloride, bromobenzene, and biphenyl-2-yllithium commercially available materials as starting chemicals to prepare fluorene instead of fluorenone as the starting materials. This synthetic route should, in principle, yield structurally perfect fluorene without fluorenone, so the problematic fluorenone emission at green region accompanied fluorene emission was well circumvented. Two substituent fluorene rings were connected through a phenyl ring followed by grafting the active anthracene group, thus improved molecular weight and thermal stability as well as elimination of intermolecular interactions to ensure high photoluminescent quantum efficiency of the anthracene moieties due to the huge hindrance of the tetrahedron fluorene dimer core. Moreover, this route avoids high-temperature and the reaction proceeds smoothly at room temperature with high yield (>95%) and purity. The detailed synthesis and characterization were described in the experimental section. The molecular structures of the target molecules were confirmed by ^1H and ^{13}C nuclear magnetic resonance (NMR), mass spectrometry, and elemental analysis.

2.2. Density functional theory calculation

Density functional theory (DFT) calculations (B3LYP; 6-31G*) were carried out to obtain information about the three-dimensional geometries and the HOMO and the lowest unoccupied molecular orbital (LUMO) energy levels distributions of the compounds. The anthracene units are significantly twisted against each other because of the tetrahedral environment of the central phenyl-substituted fluorene dimer skeleton, resulting in a non-coplanar structure in each molecule, as shown in **Fig. S1**.† Moreover, the bigger the substituent on the anthracene, the more pronounced twisted angles. These geometrical characteristics can effectively prevent intermolecular interactions between the π-systems and thus suppress molecular crystallize and improve morphological stability of thin film. The electron densities of the HOMOs and LUMOs are mainly localized on the anthracene units with a little on the aromatic rings but not on the fluorenyl skeleton, indicating no effect on the electronic structures of the anthracene units imposed by the fluorenyl skeleton through non-conjugated combination. As a result, the molecular orbital analysis clearly indicates that the substituent in 9- and/or 10-positions of anthracene does not significantly influence the blue emission nature of the anthracene unit, which proved our molecular design rational.

2.3. Thermochemical properties

The thermochemical properties of the three materials were characterized by differential scanning calorimetry (DSC) and

thermal gravimetric analysis (TGA), and all of them exhibit intrinsically amorphous characteristic. In the first heating scan, a distinct glass transition at temperature of 159 °C for DAPFB, 240.7 °C for DPAPFB, and 256.7 °C for DNAPFB, respectively, was observed, and this endothermic phase-transition still remained in the subsequently cooling and heating cycles, as shown in **Fig. S2**.† The bigger the substituent on the anthracene, the higher the T_g value. It not only hinders close packing and intermolecular interactions in the solid state, but also increases the molecular rigidity. Consequently, the introduction of 9-aryl fluorenyl into anthracene leads to reduction of the crystallization tendency and an increase in T_g. Such high T_gs make them among the highest values ever reported in the literature.[15,38] The thermal decomposition temperatures (T_d) corresponding to 5%-weight-loss reached as high as 441.4, 488.5, and 495.9 °C for DAPFB, DPAPFB, and DNAPFB, respectively. Such high T_g and T_d indicate high thermal stability of this material, which is very desirable for high performance OLEDs application. The key data of the three compounds were listed in Table 1.

To further investigate thermal and morphological stabilities of these anthracene derivatives as well as their miscibility to the dopant as possible host materials, we prepared thin films using vacuum vapor deposition method deposited on indium tin oxide (ITO) coated glass substrate of these materials and then explored their surface morphologies employing atomic force microscopy (AFM) before and after annealing. For comparison, we also fabricated ADN thin film using the same method. The topographical images revealed that our anthracene derivatives provided smooth and uniform surfaces with room-mean-square (RMS) roughness of 2.0, 1.7, and 2.3 nm for DAPFB, DPAPFB, and DNAPFB, respectively. In contrast, ADN displayed a very rougher surface with RMS of 22.9 nm, as shown in Fig. 1. Moreover, our compounds underwent negligible morphological changes after annealing at 110 °C under nitrogen for 12 h with RMS of 1.9, 2.2, and 2.2 nm for DAPFB, DPAPFB, and DNAPFB, respectively, while ADN film suffered crystallizing under thermal treating and its surface was broken. This suggested that our compounds possessing high thermal and morphological stabilities as well as good miscibility to the dopant, which can be attributed to the introduction of huge phenyl-substituted fluorene dimer as a bulky and rigid core as well as high molecular weight.

2.4. Photophysical characterization

The UV–vis absorbance and PL spectra of the three anthracene derivatives, as well as 9,10-diphenylanthracene (DPA) for comparison were measured in dilute dichloromethane solution. All of them exhibited characteristic vibronic patterns of the

Table 1 Physical properties of the anthracene derivatives

Compound	$T_g/T_m/T_d$[a]/°C	λ_{max}[b] (abs)/nm	λ_{max}[b] (em)/nm	E_g (opt.)/eV	Φ_F[c] (%)	LUMO/HOMO [d]/eV
DPA	–/248/259	356, 375, 395	411, 430	3.03	0.90	2.51/5.54
DAPFB	159/417/441	349, 367, 387	402, 423	3.03	0.61	2.59/5.59
DPAPFB	241/438/488	358, 377, 397	416, 431	3.02	0.67	2.54/5.55
DNAPFB	257/475/495	358, 377, 397	414, 433	3.02	0.96	2.55/5.55

[a] Obtained from DSC and TGA measurement. [b] Measured in dilute dichloromethane solution. [c] Φ_F values measured following a handbook using 9,10-diphenylanthracene standard ($\Phi_F = 0.90$ in cyclohexane). [d] Obtained according to the cyclic voltammetry measurement.

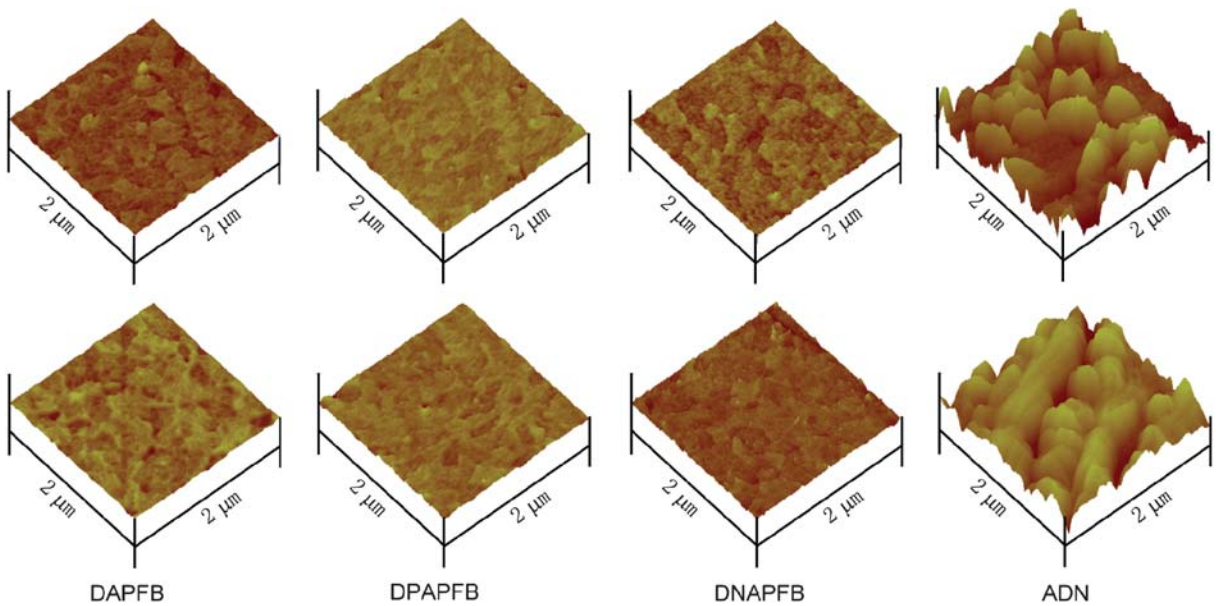

Fig. 1 Tapping mode atomic force microscopy imagine of the deposited DAPFB, DPAPFB, DNAPFB, and AND thin films doped with 10% by weight of DPAVBi surfaces; top, before heated; down, after heated at 110 °C for 12 h under nitrogen atmosphere.

isolated anthracene units, with three bands located at 355 nm, 375 nm, and 395 nm for DPA, a little of hypochromic shift of 1 nm compared with DPAPFB and DNAPFB, and 6–7 nm bathochromic shift relative to DAPFB, as shown in Fig. 2. The optical band gaps were calculated to be 3.03 eV, 3.02 eV, and 3,02 eV for DAPFB, DPAPFB, and DNAPFB, respectively, according to the maximum absorption border. The bigger the substituent aromatic ring is on the anthracene, the larger red-shift in the UV–vis spectrum. The same trend was observed in the PL spectra, since the conjugation length increases with the increasing size of the substituent aromatic rings on the anthracene from DAPFB, DPAPFB, to DNAPFB. When transferred from solution to the solid state, the UV–vis spectra only exhibited 2∼3 nm red-shifts in the absorption peaks with similar patterns of the solution's (for detail, see **Fig. S3**).† Under UV light excitation, all of the anthracene derivatives emit blue light whether in solution or in the solid state.

Further study on the PL spectra of the three anthracene derivatives in the solid state revealed that the preparation methods of films have profound effects on the photophysical properties. As for thermal deposited films, they displayed broad and featureless peaks with a maximum at 441 nm, while DPAPFB and DNAPFB showed two shoulders at 420 and 508 nm as well as very weak band at 577 nm, as shown in Fig. 2. But in the powder, they displayed characteristic emission with peak at 422 nm and shoulder at 444 nm for DAPFB, 435, 460, and 500 nm for DPAPFB, 440, 462, and 535 nm for DNAPFB, respectively. Observation of multiple bands in the PL spectra of an emitter is known and generally attributed to vibronic features or conformational isomers.[11] The observed difference between the present PL spectra was suggested to explain by the ratio of conformational isomers. It is conceivable that different conformational isomers existed in the thermal deposited film and the solid powder. As the substituent group increases form hydrogen atom, phenyl group, to naphthalene group of DAPFB, DPAPFB, and DNAPFB molecules, respectively, more atoms are combined together and thus more energetically conformational isomer, high or small, were expected to form. Compared with DAPFB molecules, DPAPFB and DNAPFB molecules, with two bigger substituent groups on the anthracene, compose more atoms and thus more energetically conformational isomer. DFT calculation results also proved a variety of conformational isomers exist. In general, the ratio of vibronic features is independent of the sample preparation. Another possible explanation for the observed difference (particularly, the evolution of emission shoulders peaking at 500∼550 nm) in the PL spectra is intramolecular interactions. Although aggregate of a kind of molecules in the solid state may also induce new emission peak characterized by broaden and weak in the PL spectrum, yet the similar UV–vis absorption spectra of the thin films and the dilute solutions exclude this possible deduction (for detail, see **Fig. S3**).† Another thing worth noting is the relatively high photoluminescent quantum yield (PLQY) in the range of 0.61 to 0.96 relative to DPA in dilute solution. High PLQY indicate eliminated interactions between molecular chromophores arising from the bulky and rigid skeleton of phenyl-substituted fluorene dimer skeleton incorporated into the anthracene at the C–9 position. Further proved our molecular design strategy rational,

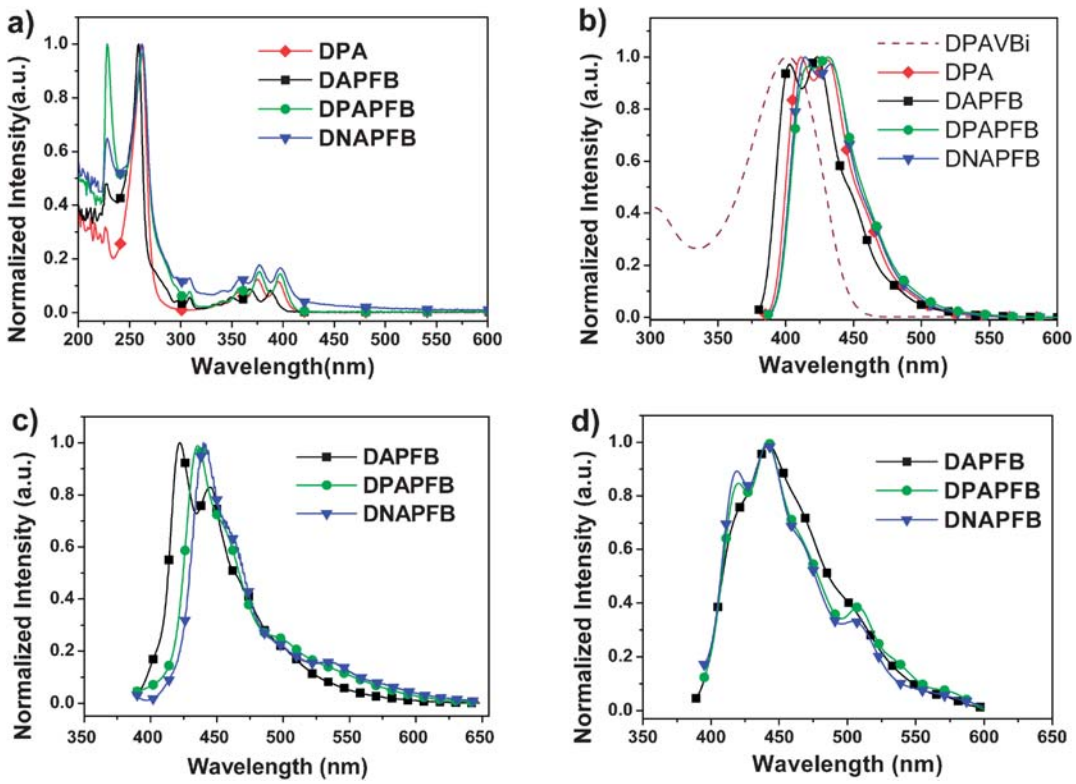

Fig. 2 UV–vis absorption (a) and PL (b) spectra of DPA, DAPFB, DPAPFB, and DNAPFB in dilute dichloromethane solution, as well as optical absorption spectrum of DPAVBi (the dash line). PL spectra of DAPFB, DPAPFB, and DNAPFB powder (c); vacuum deposited film (d).

a non-coplanar conformation not only prevents intermolecular interactions but also enables to improve the thermal and amorphous stability as well as high photoluminescent efficiency.

2.5. Electrochemical properties

In addition to the photophysical properties the electrochemical properties is also very important to determine a material characteristics and its potential application. Thus the electrochemistry of the three newly synthesized compounds was investigated by cyclic voltammetry, which was performed in a conventional three-electrode compartment cell. During the anodic oxidization voltage sweep measured in 1,2-dichloromethane, reversible oxidation peak at 1.32, 1.37, 1.32 V with onset potential at 1.19, 1.15, and 1.15 V for DAPFB, DPAPFB, and DNAPFB, respectively, were observed. Upon the cathodic voltage sweep in THF, reversible reduction peak at −2.26, −2.25, and −2.24 V with onset potentials at −1.81, −1.86, and −1.85 V for DAPFB, DPAPFB, and DNAPFB, respectively, were recorded (for detail, see **Fig. S4**).† All of them showed reversible anodic oxidation or cathodic reduction behavior during the repeat potential sweeps, indicating the potential utilization for stable hole- and electron-transporting materials.

The HOMO energy levels of DAPFB, DPAPFB, and DNAPFB were estimated from the p-doping onset potential to be −5.59, −5.55, and −5.55 eV, respectively, which is very close to that of DPA (−5.54 eV), using ferrocene as internal standard which has a value of −4.8 eV under the vacuum energy level. Accordingly, the LUMO energy levels of DAPFB, DPAPFB, and DNAPFB were calculated from the n-doping onset potential to be −2.59, −2.54, and −2.55 eV for DAPFB, DPAPFB, and DNAPFB, respectively. The electrochemical band gap (3.00, 3.01, and 3.00 eV) is, in general, well consistent with the optical band gap (3.03, 3.02, and 3.02 eV). It is also interesting to mention that the two anthracene moieties connected through the non-conjugated sp^3 hybridized carbon atom of fluorene dimer core were electrochemically oxidize or reduce simultaneously at the same potential, which further proved our molecular design concept rational. Generally speaking, the electrochemical properties and photophysical properties of DAPFB, DPAPFB, and DNAPFB in dilute solution are very similar, mirroring the anthracene unit's characteristics.

2.6. Electroluminescent properties

Encouraged by the high PLQY, high thermal stabilities, and suitable HOMO and LUMO energy levels, we fabricated devices using thermal deposition in the following configuration: ITO/α-NPB (40nm)/EML (30nm)/BCP (35nm)/Ca : Ag (100 nm), where 4,4′-bis[*N*-(1-naphthyl)-*N*-phenyl-amino]biphenyl (α-NPB) is the hole-transporting layer (HTL); EML is DAPFB, DPAPFB, or DNAPFB; 2,9-dimethyl-4,7-diphenyl-1,10-phenanthroline (BCP) used as hole-blocking and electron-transporting layer; a thin (7 Å) Ca serves as electron-injecting layer at the Ag electrode interface. The device energy level diagram was present in Fig. 3 (right). The EL spectra of DAPFB, DPAPFB, and DNAPFB show blue emissions with peaks at 460, 444, and 444 nm, respectively (see Fig. 3 left). It is interesting to note that the emission maximum of each device corresponds well to one of the maxima of the PL spectra. Similar EL spectra and PL spectra indicates the same light-emitting process derive from the decay of the singlet excitons. However, DNAPFB device, compared with DAPFB and DPAPFB devices, showed a little difference in the EL spectra, which displayed a distinct peak at around 540 nm and a shoulder at 577 nm while the other two showed negligible emission in this longer wavelength region. Although the PL spectrum of DNAPFB also was similar to its EL spectrum, yet the emission got stronger at the lower energy region, which can be attributed to the directed charge trapping effect[39] in the EL process other than the PL process. The difference between DAPFB, DPAPFB and DNAPFB in the EL spectra might be ascribed to the different low energically conformational isomers ratios changes in the electrically stimulation. Although exciplex may also generate new emission in the longer wavelength region, yet the PL spectrum of the blend films of DNAPFB with NPB or BCP showed no new emission, thus exclude this deduction (see **Fig. S5**).† All the devices showed reasonable high efficiency (Table 2); the maximum luminance efficiency reached 2.2 cd A^{-1} for DAPFB emitter, 3.2 cd A^{-1} for DPAPFB emitter, and 5.1 cd A^{-1} for DNAPFB emitter and remained very stable even at high luminance of 10000 cd m^{-2} (3.9 cd A^{-1}), which is comparable to or higher than other reported fluorescent blue-light-emitting hydrocarbons, such as anthracene derivatives[17,19,23,29,40–42] or fluoranthene compounds,[16,43] though its color purity are not idea and still need to be improved.

In order to further improve the efficiency and color purity, we adopted a host-dopant system using these materials as host and a highly fluorescent blue dye, DPAVBi, as dopant at a concentration range of 1–6% in the same device structure. The key performance characteristics of the devices are listed in Table 2. The doped DPAPFB devices exhibited bright blue emission with a peak at 460 nm and a shoulder at 492 nm, which is the intrinsic emission pattern of the dopant; no short wave emission was

Table 2 EL performance of blue OLEDs based on DAPFB, DPAPFB and DNAPFB

Light-emitting layer	EQE_{max} (%)	LE_{max}/cd A^{-1}	PE_{max} (lm W^{-1})	L_{max}[a]/cd m^{-2}	CIE[b] (x, y)	LE[c]/cd A^{-1}	PE[c] (lm W^{-1})
DAPFB	0.8	2.2	0.6	6981 (368)	0.18, 0.21	2.1	0.5
DPAPFB	1.5	3.2	1.1	12508 (713)	0.18, 0.21	2.7	0.7
DNAPFB	2.3	5.1	1.8	15559 (514)	0.24, 0.28	4.2	0.8
DPAPFB:1.1%DPAVBi	4.8	13.6	2.7	29739 (308)	0.16, 0.23	4.7	2.5
DPAPFB:1.8%DPAVBi	4.1	11.5	2.6	37120 (381)	0.16, 0.26	11.4	2.3
DPAPFB:4.0%DPAVBi	4.5	12.5	2.7	26878 (364)	0.16, 0.26	12.3	2.3
DPAPFB:6.3%DPAVBi	4.2	11.7	3.6	34795 (466)	0.16, 0.26	11.2	2.3

[a] The data in the parentheses are the corresponding current density. [b] Recorded at 12 V. [c] Values obtained at a luminance of 5000 cd m^{-2}.

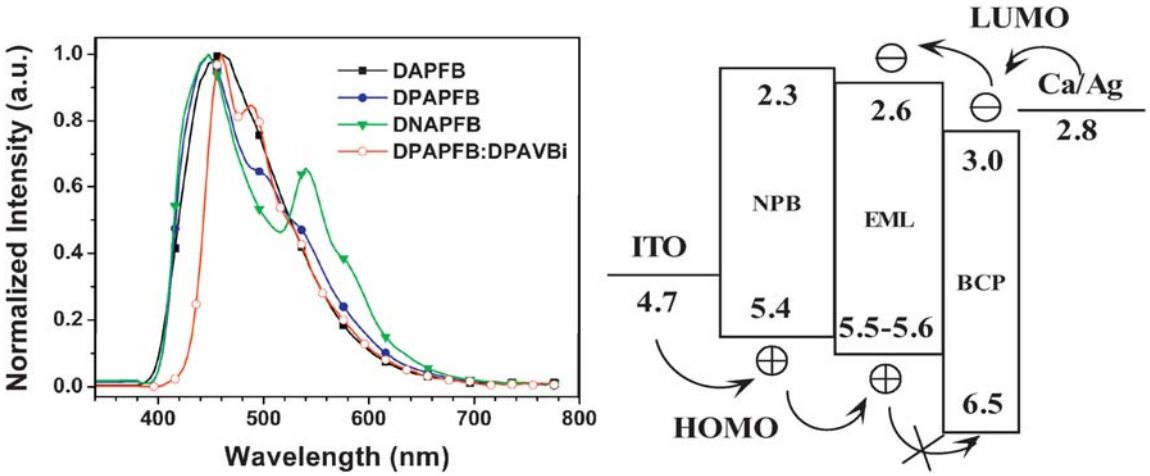

Fig. 3 EL spectra of DAPFB, DPAPFB, DNAPFB, and DPAVBi doped DPAPFB devices (left), and relative HOMO/LUMO energy levels of the materials used in the device (right).

observed indicating completely energy transfer from the host to the dopant. Furthermore, we found the emission spectra is independent of the driving voltage in the range 6–17 V, with the Commission Internationale de L'Eclairage (CIE) chromaticity coordinate values $x, y = (0.16, 0.23)$. The maximum brightness reached 37120 cd m^{-2} at a current density of 381 mA cm^{-2} corresponding to 1.8% doping concentration. Obviously, the luminance efficiencies of all the doped devices got pronounced improvement compared to the undoped ones (Fig. 4). It is worthy mentioning that the maximum efficiencies was obtained at high luminance, indicating more practical application.[44] For example, the 1.1% doped device showed a maximum luminance efficiency of 13.6 cd A^{-1} (corresponding to an external quantum efficiency of 4.8%) at brightness over 2000 cd m^{-2}, more than two-fold enhancement over spirobifluorene-linked bisanthracene derivatives as host materials (4.9 cd A^{-1}).[24] As for DNAPFB host, it exhibited even higher efficiencies than DPAPFB host (for details, see Table 3). The maximum luminance efficiency reached 14.8 cd A^{-1} (corresponding external quantum efficiency of 3.5%) and the maximum brightness is 53504 cd m^{-2} (Fig. 5). In addition, the current efficiencies show only a mild decrease as the luminance increase. For example, the device based on DANPFB host with 10% doping concentration shows a slightly decrease in efficiency to 13.3 cd A^{-1} when the luminance increased to 5000 cd m^{-2}.

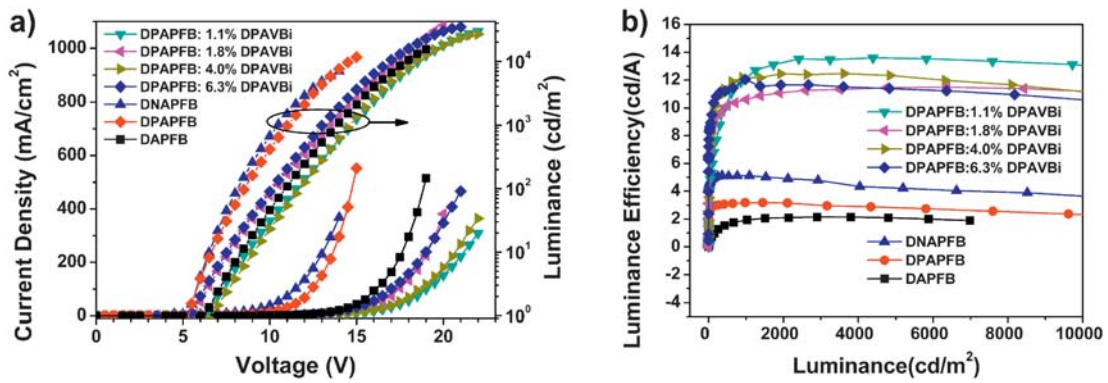

Fig. 4 Current density–voltage–luminance characteristics (a) and luminance efficiency as a function of luminance (b) for the DAPFB, DPAPFB and DNAPFB based devices.

Table 3 EL properties characteristics of DPAVBi doped DNAPFB emitter

Light-emitting layer	EQE_{max} (%)	LE_{max}/cd A^{-1}	PE_{max} (lm W^{-1})	CIE[a] (x, y)	L_{max}[b]/cd m^{-2}	LE[c]/cd A^{-1}	PE[c] (lm W^{-1})
DNAPFB:6%DPAVBi	3.0	10.4	4.6	0.32, 0.40	16474 (179)	10.0	2.0
DNAPFB:8%DPAVBi	3.3	13.7	4.8	0.32, 0.41	53504 (607)	13.2	2.9
DNAPFB:10%DPAVBi	3.5	14.8	5.3	0.32, 0.41	50248 (623)	13.3	2.5
DNAPFB:20%DPAVBi	2.7	11.4	6.9	0.33, 0.42	33026 (385)	10.7	1.9

[a] Recorded at 12 V. [b] The data in the parentheses are the corresponding current density. [c] Recorded at a luminance of 5000 cd m^{-2}.

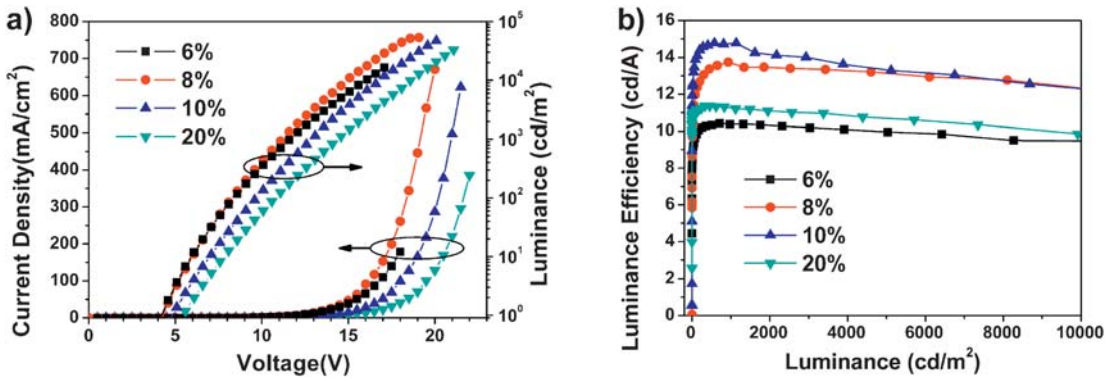

Fig. 5 Current density–voltage–luminance characteristics (a) and luminance efficiency as a function of luminance (b) for the DPAVBi doped DNAPFB devices.

Interestingly, we found the DNAPFB host incorporating a sky-blue dopant DPAVBi emits white light, which is never reported in the literatures. The maximum brightness and luminance efficiency are also high, superior to that of other conventional fluorescent white OLEDs based on anthracene blue host and pyran derivatives orange dye two-spectrum single layer white light-emitting system.[22,45] This kind of white fluorescent OLEDs may be very promising, considering its over performance and simple device architecture: a three-layer device structure, which is consist of hole-transporting layer, emissive layer, and hole-blocking/electron transporting layer without electrode modification or complicate device structural engineering.

As for the EL spectra of doped DNAPFB devices, however, they displayed another peak at 540 nm and a shoulder at 577 nm, in addition to the short waves at 460 and 492 nm which is the intrinsic emission of the dopant, very different from DPAPFB host devices, which showed white emission other than blue light of DPAPFB host devices, as shown in Fig. 6. Like the non-doped EL spectrum, this low energy emissions at 540 nm and 577 nm are also occurred in the doped devices, which is well consistent with the PL spectra of DNAPFB in the solid state, only the relative intensity getting stronger, and we found this low energy emission can not be eliminated even at high doping concentration, which is not difficult to understand. In a doped host–guest system, Förster energy transfer can take place from the higher energy emissive host to the lower energy emissive dopant, while the lower energy section can not transfer its energy to the dopant exothermically and remained; that is the emission peak of DNAPFB at 444 nm is energetically transferred to the dopant while the lower energy emission band at 540 nm and 577 nm did not transfer their energy to the dopant. And due to the lower energy sites competed with the dopant to get excitons, energy transfer is more favorable to transfer to the lower emission site in addition to directly charge trapping by the lower emission sites, so the emission at longer wavelength region get stronger in the doped system than in the non-doped system and became dominant. This demonstrated why we can not get blue emission by doping DPAVBi into DNAPFB host. Fortunately, by employing these low energy emissions and a sky-blue dopant controlled at suitable doping level we got white emission. The CIE chromaticity coordinates vary from (0.32, 0.38) to (0.32, 0.41) in the driving voltage range of 9–17 V (corresponding brightness of 77–13608 cd m^{-2}), very close to the balanced equienergy white point of (0.33, 0.33) (see the inset of Fig. 6). The negligible variation in the CIE values and EL efficiency can be attributed to the balanced recombination and emission of the excitons well confined in the single emissive layer of the DNAPFB and DPAVBi binary blend emitting system.

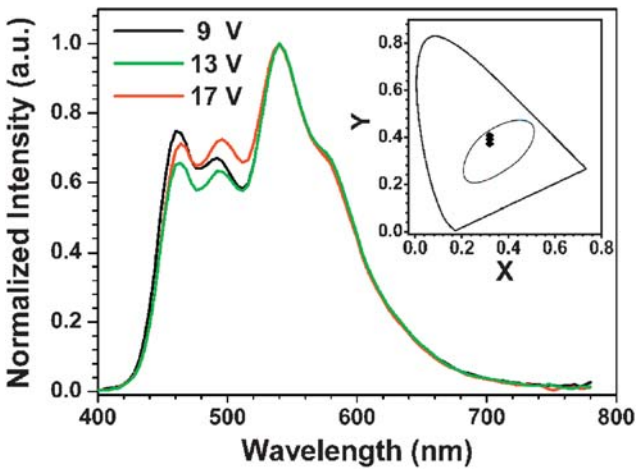

Fig. 6 EL spectra of DPAVBi doped DNAPFB device at a range of driving voltage (inset is the CIE coordinate).

For comparison, we also fabricated another device based on ADN host in the same device architecture with the same doping concentration, and found the maximum efficiency is only 8.5 cd A^{-1} (CIE coordinates = (0.21, 0.37), EQE = 3.2%). A similar device configuration combining the organic materials of DPAVBi and ADN showed comparable EL efficiency of 7.96 cd A^{-1} with CIE$_{x,y}$ (0.28, 0.34) reported by Lee *et al.*[46] Further improving its EL efficiency to 9.7 cd A^{-1} with CIE$_{x,y}$ (0.16, 0.32) by adding CF_x as the hole injection layer was achieved by Lee *et al.*[47] Compared with ADN host material, our host materials greatly improved efficiency and color purity. In general, OLED performance is described as a product of four factors: (1) carrier balance factor, (2) exciton formation ratio, (3) photoluminescent quantum yield (PLQY), and (4) light out-coupling factor. Among them, there seem to be mainly two factors, (1) and (3), to determine these device performances. In energy level point of view, both DNAPFB and DPAPFB have suitable

HOMO and LUMO energy levels, with value at −5.51 and −2.56 eV, respectively, well encompassed those of the dopant, thus facilitate charge injecting and transporting into the dopant and well confined excitons on the dopant. Moreover, there are good spectral overlaps between the absorption spectrum of the dopant and the PL spectra of the anthracene derivatives, thus ensured efficient Förster energy transfer from the host to the dopant (Fig. 2). Furthermore, the high PLQY of the host materials partly accounts for the high efficiency of the doped or undoped devices. At last, this host-dopant system possesses exceptional miscibility, film-forming ability, and morphology stability as revealed by the AFM surface morphology measurement.

3. Conclusions

In conclusion, we have successfully designed and synthesized a new series of anthracene derivatives *via* simple Suzuki coupling reaction by incorporating a rigid and bulky tetrahedral molecular skeleton, featuring a phenyl-substituted fluorene dimer as bulky and rigid core and anthracene as a functional active group. The non-coplanar molecular structure resulting from the tetrahedral environment of the phenyl-substituted fluorene dimer and aryl-substitution group of the anthracene units provide steric hindrance that prevents close packing of the molecules in the solid state and also enables to form high thermal and morphological stable film, high PLQY, and well miscibility with the dopant. Devices based on these anthracene derivatives show bright blue emission with color purity and high efficiency up to 5.1 cd A^{-1} in an undoped device structure. Moreover, the doped DPAPFB-based devices exhibit outstanding efficiencies, with maximum luminance efficiency of 13.6 cd A^{-1} (EQE 4.8%) at 43.1 mA cm^{-2}, corresponding to a brightness of 5820.9 cd m^{-2}. Furthermore, we have fabricated highly efficient white fluorescent OLEDs based on incomplete energy transfer between DNAPFB and DPAVBi binary host-gust emitter system in a doped device configuration with maximum EL efficiency of 14.8 cd A^{-1} and maximum brightness of 53504 cd m^{-2} as well as stable $CIE_{x,y}$ value of (0.33, 0.38). The comprehensive physical and chemical characteristics examination results indicate that our molecular design is successful and our anthracene derivatives are promising candidates for photoelectronics application.

4. Experimental

4.1. Synthesis

All starting materials were obtained from commercial suppliers and used without further purification. 9-Bromoanthracene, isophthaloyl dichloride, and $AlCl_3$ were purchased from Alfa Aesar. n-Butyllithium was purchased from Merck. 2-Isopropoxy-4,4,5,5-tetramethyl-[1,3,2]dioxaborolane was purchased from Aldrich. All the solvents were distilled before use according to literature procedure (fee detailed synthesis process, see ESI†)

4.2. Characteristics

^1H NMR and ^{13}C NMR measurements were carried out on a Bruker DMX 400 NMR spectrometer. MS spectrometry (MALDI-TOF-MS) was determined on a Bruker BIFLEX III mass spectrometer. Elemental analyses were carried out on a Carlo-Erba 1160 elemental analyzer. Thermogravimetric analyses (TGA) were carried out using a Perkin-Elmer thermogravimeter (Model TGA7) under a dry nitrogen gas flow at a heating rate of 10 °C min^{-1}. Glass transition temperatures (T_g) and melting phase-transition temperature (T_m) were determined by differential scanning calorimetry (DSC) at a heating rate of 10 °C min^{-1} using a Perkin-Elmer differential Scanning calorimeter (DSC7). The cyclic voltammetry (CV) characterization was performed on CHI 600C Electrochemical Workstation in a conventional three-electrode cell using dichloromethane for anodic sweep (THF for cathodic sweep) containing 0.1 M n-Bu_4NPF_6 as supporting electrolyte *versus* Ag/AgCl reference electrode, platinum disk as working electrode, and platinum wire as counter electrode. UV–vis absorption and fluorescence spectra were collected with a Hitachi U–3010 and Hitachi F–4500 spectrophotometer, respectively.

4.3. Fluorescence quantum yield measurements

The Φ_F values in solution were measured following a general method using 9,10-diphenylanthracene, which has a absolute Φ_F values of 0.9 in cyclohexane, as the standard.[48] Dilute solutions of DAPFB, DPAPFB, and DNAPFB in cyclohexane solvent were used for recording the fluorescence spectra. Sample solutions were degassed for 15 min and taken in quartz cuvettes to record the absorption spectra, which the absorption intensity of the excitation wavelength was adjusted at around 0.05. The fluorescence spectra of each were excited at the same wavelength and recorded 5 times, and an average value of integrated areas of fluorescence was used for the calculation of Φ_F values. The refractive indices of solvents were used for the correlation of the Φ_F values.

4.4. Device fabrication and measurements

In a general procedure, indium-tin oxide (ITO)-coated glass substrates were etched, patterned, and washed with detergent, deionized water, acetone, and ethanol in turn. All the organic layers were successively deposited by vacuum deposition onto the ITO coated glass substrates at a pressure of 8×10^{-5} Pa. In all devices, a thin (7 Å) Ca layer serves as electron-injecting layer at the Ag electrode interface and a 100-nm-thick Ag capping layer were deposited through a shadow mask. The active area of device was 5 mm^2. EL spectra and chromaticity coordinates were measured with a SpectraScan PR650 photometer. Current density–voltage–luminance (*J–V–L*) measurements were recorded simultaneously using a Keithley 4200 semiconductor parameter analyzer and a Newport multifunction 2835–C optical meter, with luminance was measured in the forward direction. All device characterizations were carried out under ambient laboratory air at room temperature.

Acknowledgements

We acknowledge financial support from the National Natural Science Foundation of China (20825208, 60736004, 20721061), the National Major State Basic Research Development Program (2006CB806203, 2006CB932103, 2009CB623603), and the Chinese Academy of Sciences.

Notes and references

1 C. W. Tang and S. A. Vanslyke, *Appl. Phys. Lett.*, 1987, **51**(12), 913.
2 M. A. Baldo, M. E. Thompson and S. R. Forrest, *Nature*, 2000, **403**(6771), 750.
3 S. R. Forrest, *Nature*, 2004, **428**(6986), 911.
4 M. Ikai, S. Tokito, Y. Sakamoto, T. Suzuki and Y. Taga, *Appl. Phys. Lett.*, 2001, **79**(2), 156.
5 C. Adachi, M. A. Baldo, S. R. Forrest and M. E. Thompson, *Appl. Phys. Lett.*, 2000, **77**(6), 904.
6 C. Adachi, M. A. Baldo, M. E. Thompson and S. R. Forrest, *J. Appl. Phys.*, 2001, **90**(10), 5048.
7 C. Hosokawa, H. Higashi, H. Nakamura and T. Kusumoto, *Appl. Phys. Lett.*, 1995, **67**(26), 3853.
8 H. C. Li, Y. P. Lin, P. T. Chou, Y. M. Cheng and R. S. Liu, *Adv. Funct. Mater.*, 2007, **17**(4), 520.
9 M. T. Lee, C. H. Liao, C. H. Tsai and C. H. Chen, *Adv. Mater.*, 2005, **17**(20), 2493.
10 Y. Liu, J. H. Guo, J. Feng, H. D. Zhang, Y. Q. Li and Y. Wang, *Appl. Phys. Lett.*, 2001, **78**(16), 2300.
11 H. T. Shih, C. H. Lin, H. H. Shih and C. H. Cheng, *Adv. Mater.*, 2002, **14**(19), 1409.
12 C. C. Wu, Y. T. Lin, H. H. Chiang, T. Y. Cho, C. W. Chen, K. T. Wong, Y. L. Liao, G. H. Lee and S. M. Peng, *Appl. Phys. Lett.*, 2002, **81**(4), 577.
13 F. Steuber, J. Staudigel, M. Stossel, J. Simmerer, A. Winnacker, H. Spreitzer, F. Weissortel and J. Salbeck, *Adv. Mater.*, 2000, **12**(2), 130.
14 C. H. Chen, F. I. Wu, C. F. Shu, C. H. Chien and Y. T. Tao, *J. Mater. Chem.*, 2004, **14**(10), 1585.
15 S. L. Tao, Z. K. Peng, X. H. Zhang, P. F. Wang, C. S. Lee and S. T. Lee, *Adv. Funct. Mater.*, 2005, **15**(10), 1716.
16 R. C. Chiechi, R. J. Tseng, F. Marchioni, Y. Yang and F. Wudl, *Adv. Mater.*, 2006, **18**(3), 325.
17 Y. Kan, L. D. Wang, L. Duan, Y. C. Hu, G. S. Wu and Y. Qiu, *Appl. Phys. Lett.*, 2004, **84**(9), 1513.
18 K. Danel, T. H. Huang, J. T. Lin, Y. T. Tao and C. H. Chuen, *Chem. Mater.*, 2002, **14**(9), 3860.
19 T. Karatsu, R. Hazuku, M. Asuke, A. Nishigaki, S. Yagai, Y. Suzuri, H. Kita and A. Kitamura, *Org. Electron.*, 2007, **8**(4), 357.
20 S. K. Kim, B. Yang, Y. Ma, J. H. Lee and J. W. Park, *J. Mater. Chem.*, 2008, **18**(28), 3376.
21 Y. H. Kim, H. C. Jeong, S. H. Kim, K. Y. Yang and S. K. Kwon, *Adv. Funct. Mater.*, 2005, **15**(11), 1799.
22 P. I. Shih, C. Y. Chuang, C. H. Chien, E. W. G. Diau and C. F. Shu, *Adv. Funct. Mater.*, 2007, **17**(16), 3141.
23 S. L. Tao, S. D. Xu and X. H. Zhang, *Chem. Phys. Lett.*, 2006, **429** (4–6), 622.
24 W. J. Shen, R. Dodda, C. C. Wu, F. I. Wu, T. H. Liu, H. H. Chen, C. H. Chen and C. F. Shu, *Chem. Mater.*, 2004, **16**(5), 930.
25 Y. H. Kim, D. C. Shin, S. H. Kim, C. H. Ko, H. S. Yu, Y. S. Chae and S. K. Kwon, *Adv. Mater.*, 2001, **13**(22), 1690.
26 K. S. Kim, Y. M. Jeon, J. W. Kim, C. W. Lee and M. S. Gong, *Org. Electron.*, 2008, **9**(5), 797.
27 C. H. Wu, C. H. Chien, F. M. Hsu, P. I. Shih and C. F. Shu, *J. Mater. Chem.*, 2009, **19**(10), 1464.
28 Y. Y. Lyu, J. Kwak, O. Kwon, S. H. Lee, D. Kim, C. Lee and K. Char, *Adv. Mater.*, 2008, **20**(14), 2720.
29 J. M. Shi and C. W. Tang, *Appl. Phys. Lett.*, 2002, **80**(17), 3201.
30 B. D. Ding, W. Q. Zhu, X. Y. Jiang and Z. L. Zhang, *Curr. Appl. Phys.*, 2008, **8**(5), 523.
31 Y. Kim, S. Kwon, D. Yoo, M. F. Rubner and M. S. Wrighton, *Chem. Mater.*, 1997, **9**(12), 2699.
32 S. Tokito, H. Tanaka, K. Noda, A. Okada and Y. Taga, *Appl. Phys. Lett.*, 1997, **70**(15), 1929.
33 P. I. Shih, C. H. Chien, T. I. Wu and C. F. Shu, *Adv. Funct. Mater.*, 2007, **17**(17), 3514.
34 K. T. Wong, Y. M. Chen, Y. T. Lin, H. C. Su and C. C. Wu, *Org. Lett.*, 2005, **7**(24), 5361.
35 P. I. Shih, C. L. Chiang, A. K. Dixit, C. K. Chen, M. C. Yuan, R. Y. Lee, C. T. Chen, E. W. G. Diau and C. F. Shu, *Org. Lett.*, 2006, **8**(13), 2799.
36 S. H. Ye, Y. Q. Liu, C. A. Di, H. X. Xi, W. P. Wu, Y. G. Wen, K. Lu, C. Y. Du, Y. Liu and G. Yu, *Chem. Mater.*, 2009, **21**(7), 1333.
37 S. Y. Cho, A. C. Grimsdale, D. J. Jones, S. E. Watkins and A. B. Holmes, *J. Am. Chem. Soc.*, 2007, **129**, 11910.
38 Q. X. Tong, S. L. Lai, M. Y. Chan, K. H. Lai, J. X. Tang, H. L. Kwong, C. S. Lee and S. T. Lee, *Chem. Mater.*, 2007, **19**(24), 5851.
39 J. M. Lupton, P. Schouwink, P. E. Keivanidis, A. C. Grimsdale and K. Mullen, *Adv. Funct. Mater.*, 2003, **13**(2), 154.
40 S. Tao, Y. C. Zhou, C. S. Lee, S. T. Lee, D. Huang and X. H. Zhang, *J. Phys. Chem. C*, 2008, **112**(37), 14603.
41 C. H. Chien, C. K. Chen, F. M. Hsu, C. F. Shu, P. T. Chou and C. H. Lai, *Adv. Funct. Mater.*, 2009, **19**(4), 560.
42 Y. Kan, L. D. Wang, Y. D. Gao, L. Duan, G. S. Wu and Y. Qiu, *Synth. Met.*, 2004, **141**(3), 245.
43 R. J. Tseng, R. C. Chiechi, F. Wudl and Y. Yang, *Appl. Phys. Lett.*, 2006, **88**(9), 093512.
44 W. S. Jeon, T. J. Park, S. Y. Kim, R. Pode, J. Jang and J. H. Kwon, *Appl. Phys. Lett.*, 2008, **93**(6), 063303.
45 J. H. Jou, Y. S. Chiu, R. Y. Wang, H. C. Hu, C. P. Wang and H. W. Lin, *Org. Electron.*, 2006, **7**(1), 8.
46 T. W. Lee, T. Noh, B. K. Choi, M. S. Kim, D. W. Shin and J. Kido, *Appl. Phys. Lett.*, 2008, **92**(4), 043301.
47 M. T. Lee, H. H. Chen, C. H. Liao, C. H. Tsai and C. H. Chen, *Appl. Phys. Lett.*, 2004, **85**(15), 3301.
48 J. C. Scaiano *Handbook of Organic Photochemistry*; CRC Press: Boca Raton, Florida, 1989; Vol. 1. pp 233.

